1 # Mutually opposing activity of PIN7 splicing isoforms is required

2 # for auxin-mediated tropic responses in *Arabidopsis thaliana*

3

4 **Ivan Kashkan[1,2], Mónika Hrtyan[2], Roberta Filepová[1], Zuzana Vondráková[1], Jan**

5 **Hejátko[2], Sibu Simon[1], Debbie Rombaut[3,4], Thomas B. Jacobs[3,4], Mikko J. Frilander[5],**

6 **Jiří Friml[6], Jan Petrášek[1], Kamil Růžička[1,2,7,*]**

7

8 [1]*Laboratory of Hormonal Regulations in Plants, Institute of Experimental Botany, Czech Academy of*

9 *Sciences, 16502 Prague, Czech Republic*

10 [2]*Functional Genomics and Proteomics of Plants, Central European Institute of Technology and*

11 *National Centre for Biomolecular Research, Masaryk University, 62500 Brno, Czech Republic*

12 [3]*Department of Plant Biotechnology and Bioinformatics, Ghent University, 9052 Ghent, Belgium*

13 [4]*VIB Center for Plant Systems Biology, 9052 Ghent, Belgium*

14 [5]*Institute of Biotechnology, University of Helsinki, 00014 University of Helsinki, Finland*

15 [6]*Institute of Science and Technology (IST Austria), 3400 Klosterneuburg, Austria*

16 [7]*Lead Contact*

17

18 [*]Correspondence: kamil.ruzicka@ueb.cas.cz

19

20 **SUMMARY**

21   Advanced transcriptome sequencing has revealed that the majority of eukaryotic genes

22 undergo alternative splicing (AS). Nonetheless, limited effort has been dedicated to

23 investigating the functional relevance of particular splicing events, even those in the key

24 developmental and hormonal regulators. Here we reveal, in the plant model *Arabidopsis*

25 *thaliana*, that the *PIN7* gene, which encodes a polarly localized transporter for the

26 phytohormone auxin, produces two evolutionarily conserved transcripts. These isoforms

27 PIN7a and PIN7b, differing in a 4 amino acid motif, are present at nearly equal levels in most

28 cells, except some early developing tissues where the expression of PIN7b is moderately

29 prevalent. Both proteins also transport auxin with similar capacity and directionality.

30 However, only *PIN7a* but not *PIN7b* cDNA rescues the phenotypes associated with the *pin7*

31 knock-out mutation, consistent with their differences in the subcellular trafficking and

32 dynamics at the plasma membrane. Further phenotypic analyses suggested a joint, mutually

33 opposing activity of both isoforms as being required for correct seedling apical hook

34 formation and auxin-mediated tropic responses. These results establish alternative splicing of

35 the PIN family as an evolutionary conserved, functionally relevant mechanism, taking part in

36 the auxin-mediated plant development.

37

38 **KEYWORDS**

41

42 **INTRODUCTION**

43   Auxin is an essential phytohormone, which plays a role in nearly all aspects of plant

44 development. To flexibly adapt to rapidly changing environmental cues, directional auxin

45 transport represents a highly dynamic means for triggering downstream morphogenetic

46 processes. PIN FORMED (PIN) auxin efflux carriers are among the key regulators in this

47 respect. Many efforts in the past years uncovered several mechanisms operating

48 transcriptionally or post-translationally on the capacity and directionality of PIN-mediated

49 transport. However, little progress has been made in exploring the contribution of post-

50 transcriptional regulation (Adamowski and Friml, 2015; Hrtyan et al., 2015).

51   Advances in high throughput sequencing have revealed unexpected complexity within

52 eukaryotic transcriptomes by alternative splicing (AS). Although the majority of AS

53 transcripts may be functionally neutral (Darracq and Adams, 2013; Reddy et al., 2013; Tress

54   et al., 2017; Blencowe, 2017; Mei et al., 2017), several detailed studies have highlighted a

55   plausible role for numerous AS events in physiologically relevant contexts, including those

56   involved in plant developmental and hormonal pathways (Staiger and Brown, 2013; Hrtyan et

57   al., 2015; Shang et al., 2017; Szakonyi and Duque, 2018). Earlier works have described

58   auxin-related defects resulting from the aberrant function of several regulators of AS (Kalyna

59   et al., 2003; Casson et al., 2009; Retzer et al., 2014; Tsugeki et al., 2015; Hrtyan et al., 2015;

60   Bazin et al., 2018). AS changes subcellular localization of the auxin biosynthetic gene

61   *YUCCA 4* (Kriechbaumer et al., 2012) and differential splicing of an exitron (Marquez et al.,

62   2015) inside the *AUXIN RESPONSE FACTOR 8* results in developmental changes of

63   generative organs (Ghelli et al., 2018). AS of the Major Facilitator Superfamily transporter

64   ZIFL1 interferes with auxin transport, influencing the stability of PINs on the plasma

65   membrane (PM) (Remy et al., 2013). These lines of evidence suggest that AS is an important

66   player in auxin-dependent processes. However, no coherent functional model of any auxin-

67   related AS event has been provided so far.

68   Here, we characterize AS of the *PIN7* gene in *Arabidopsis thaliana*. PIN7 is, together

69   with PIN3 and PIN4, a member of the PIN3 clade of PIN auxin efflux carriers (Bennett et al.,

70   2014), which are required for a broad range of morphogenetic and tropic processes

71   (Adamowski and Friml, 2015). We reveal that AS influences the dynamics of the PIN7

72   protein on the PM. We also demonstrate that the coordinated action of both splice variants is

73   required for fine-tuning auxin-mediated tropic responses and during apical hook development.

74

75   **RESULTS**

76   *Arabidopsis PIN7* **and** *PIN4* **produce two evolutionarily conserved AS transcripts**

77   Our previous survey (Hrtyan et al., 2015) revealed that several genes involved in

78   auxin-dependent processes undergo AS. Among them, closely related paralogs from the *PIN3*

79   clade of auxin transporters, *PIN4* and *PIN7* (but not *PIN3*), are regulated by the same type of

80   AS (Petrasek et al., 2006; Bennett et al., 2014; Hrtyan et al., 2015). The resulting transcripts,

81   denoted as *a* and *b*, differ in the position of the AS donor site in the first intron (Figure 1A).

82   The differentially spliced region corresponds to a four amino acid motif inside the large

83   internal hydrophilic loop (Ganguly et al., 2014; Nodzyński et al., 2016) of the integral PM

84   transporter (Figure 1A and 1B). We examined the quantities of individual reads spanning the

85   exon junctions in the respective region from the *Arabidopsis* root tip and in several other

86   available transcriptomes from different tissues and organs (Klepikova et al., 2016; Cheng et

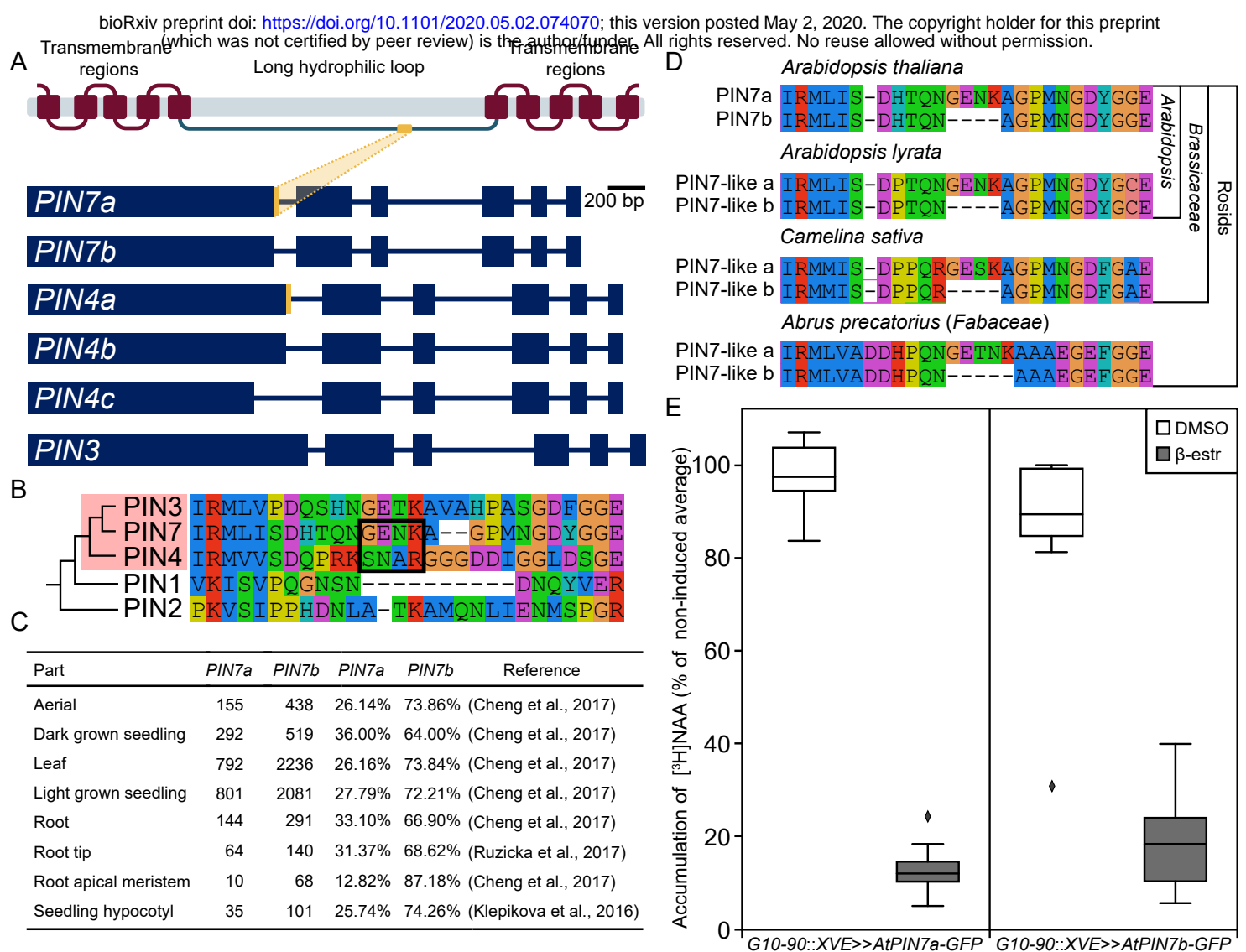87   al., 2017; Ruzicka et al., 2017) (Figures 1C and Supplemental Figure 1A). We found that both

3

Figure 1. Alternative splicing (AS) of the Arabidopsis thaliana PIN7 and PIN4 leads to two evolutionary conserved functional transcripts.

(A) Scheme of coding regions of the PIN3 clade genes in Arabidopsis thaliana. The alternative donor splice site at the end of the first exon of PIN7 and PIN4, respectively, but not PIN3, results in two transcripts differing in 12 nucleotides. This sequence (orange) corresponds to the protein motif, located in the long internal hydrophilic loop of the transporter. There is also an additional PIN4c transcript present in publicly available transcriptomes.

(B) Amino acid alignment of the region around the 4-amino acid motif changed by AS in the PIN3 clade proteins (boxed in pink) in Arabidopsis thaliana, including the closest PIN paralogs.

(C) Table shows the number of RNA-seq reads spanning the exon1-exon2 junction corresponding to the detected PIN7 transcripts in selected Arabidopsis thaliana tissue sources. Their ratio was calculated as a percentage of total reads mapped to this area as assessed from the genome browser graphic interface.

(D) Protein sequence alignment showing the conservation of AS in the PIN3 clade of auxin transporters among rosids.

(E) Accumulation of [3H]NAA in BY-2 cells following induction of Arabidopsis thaliana G10-90::XVE>>AtPIN7a-GFP and G10-90::XVE>>AtPIN7b-GFP cDNAs with 1 μM β-estradiol. [3H]NAA accumulations within the observed period show no difference between both tested isoforms. The values shown in box plots were normalized to the average maximum of the [3H]NAA accumulation rates in the non-induced lines. Middle line shows median, the box corresponds to the 25% and 75% quartiles, the whiskers represent minima and maxima (n = 9).

See also Supplemental Figure 1.

4

88   *PIN4*- and *PIN7a* and *b* transcripts are expressed abundantly in all tissues, independently on

89   the data set inspected. Besides these AS events, we also identified a minor *PIN4c* (Marquez et

90   al., 2012; Hrtyan et al., 2015) splice isoform (but not corresponding *PIN7c*), which comprised

91   around 3-7% of the *PIN4* exon1-exon2 spanning reads (Figures 1A and Supplemental Figure

92   1A). Other occasionally observed transcripts (also corresponding to the other exon junctions)

93   were not repetitively seen among different RNA-seq data sets. It thereby appears that *PIN7*

94   and *PIN4* are processed into two and three transcripts, respectively, and that *PIN7a* and *b* (or

95   *PIN4a* and *b*) are expressed in most of the plant organs at comparable or nearly similar levels.

96   Functionally relevant AS events are commonly evolutionarily conserved (Keren et al.,

97   2010; Reddy et al., 2013), therefore we sought for available validated transcripts to determine

98   whether similar splicing events occur in orthologous *PIN3* clade genes in other dicot species

99   (Bennett et al., 2014; O'Leary et al., 2016). We found examples of such mRNAs besides

100   members of the *Brassicaceae* family, for instance, also in *Abrus precatorius* (*Fabaceae*),

101   which documents the conservation of this AS event in rosids, a plant clade which diversified

102   more than 100 million years ago (Li et al., 2019) (Figure 1D). *PIN4c* did not show any deeper

103   evolutional conservation. Thus, at least some genes of the *PIN3* clade are regulated by the

104   same type of AS, across several plant families, which suggests that these AS events may have

105   a relevant biological function.

106

107   **PIN7a and PIN7b transport auxin with comparable rates in tobacco cells**

108   To test whether both protein isoforms indeed function as auxin transporters, we

109   exemplified this on the expression of the *PIN7a* and *b* cDNA variants tagged with GFP,

110   respecting the design of the original *PIN7-GFP* construct (Blilou et al., 2005), under the

111   control of the β-estradiol-driven promoter in tobacco BY-2 cells (Petrasek et al., 2006; Müller

112   et al., 2019). Following induction of both transgenes, we observed a comparable decrease of

113   radioactive-labeled auxin accumulation inside the BY-2 cells (Figure 1E) and the time course

114   of the auxin accumulation drop appeared to be similar for both constructs (Supplemental

115   Figure 1B), in accord to that of *PIN7a* cDNA, examined previously (Petrasek et al., 2006).

116   These experiments reveal that *PIN7a* and *PIN7b* code for true auxin exporters, which

117   transport auxin at similar rates in tobacco cell cultures.

118

119   **AS changes subcellular dynamics of PIN proteins**

120   Polarity and dynamic intracellular trafficking are essential functional attributes of

121   PINs (Adamowski and Friml, 2015). We expressed fluorescently-tagged cDNA versions of

5

122   the respective *PIN7* and *PIN4* transcripts under their native promoters in *Arabidopsis*

123   *thaliana*. Their overall expression patterns resembled those of the *PIN7-GFP* and *PIN4-GFP*

124   lines made on the basis of the genomic sequence (Supplemental Figures 2A-2D). At the

125   cellular level, the protein isoform localization did not largely differ from each other in terms

126   of polarity or general subcellular localization in the root tip (Figure 2A). Thus, at a given

127   resolution, it appears that the motif substituted during AS does not change the basic

128   subcellular localization or expression pattern of both PIN7 and PIN4 proteins.

129   The anterograde trafficking of proteins towards PM can be effectively blocked by the

130   fungal toxin brefeldin A (BFA). It leads to internal accumulation of the membrane-bound

131   PINs into characteristic BFA bodies (Geldner et al., 2001; Kleine-Vehn et al., 2010). During

132   time-lapse imaging, we observed that while PIN7a-GFP accumulated readily in these

133   intracellular aggregates, PIN7b-RFP formed less pronounced aggregates, co-localizing with

134   PIN7a-GFP incompletely (Figures 2A and 2B; Supplemental Figure 2E). To exclude that the

135   fluorescent tag influences the sensitivity of the PIN7 intracellular trafficking caused by BFA,

136   we compared the response of PIN7a-GFP with additionally generated PIN7b-GFP cDNA

137   expressing lines. We observed that the BFA mediated aggregation of PIN7b-GFP indeed

138   showed a moderate delay, compared with PIN7a-GFP (Figure 2C). These observations

139   suggest that the PIN7 isoforms differ in the speed of their intracellular trafficking pathways or

140   delivery to the PM and the choice of the tag does not appear to interfere significantly with the

141   subcellular dynamics of PIN7.

142   PIN polarity does not seem to strictly require the cytoskeleton (Glanc et al., 2018), but

143   subcellular PIN trafficking has been proposed to be mediated by two distinct pathways

144   (Geldner et al., 2001; Glanc et al., 2018). The first is dependent on actin filaments

145   (cytochalasin D-sensitive) and occurs in most cells of the root meristem. The second

146   (oryzalin-sensitive) utilizes microtubules and is linked with cytokinesis. Drugs that

147   depolymerize actin filaments (cytochalasin D) and tubulin (oryzalin) (Geldner et al., 2001;

148   Kleine-Vehn et al., 2008b) showed only little effect on the intracellular localization of both

149   PIN7 isoforms when applied alone (Supplemental Figures 2F and S2G). Pretreatment with

150   cytochalasin D prevented the formation of the BFA bodies (Geldner et al., 2001) containing

151   both PIN7 isoforms (Figure 2D). Yet, when we applied oryzalin prior to the BFA treatment,

152   the BFA compartments containing PIN7a-GFP and PIN7b-RFP associated in only very

153   weakly co-localizing structures (Figure 2E).

154   Next, we tested how the cytoskeleton is involved in the trafficking of both PIN7

155   isoforms from the BFA bodies to the PM by washing out BFA with cytochalasin D or
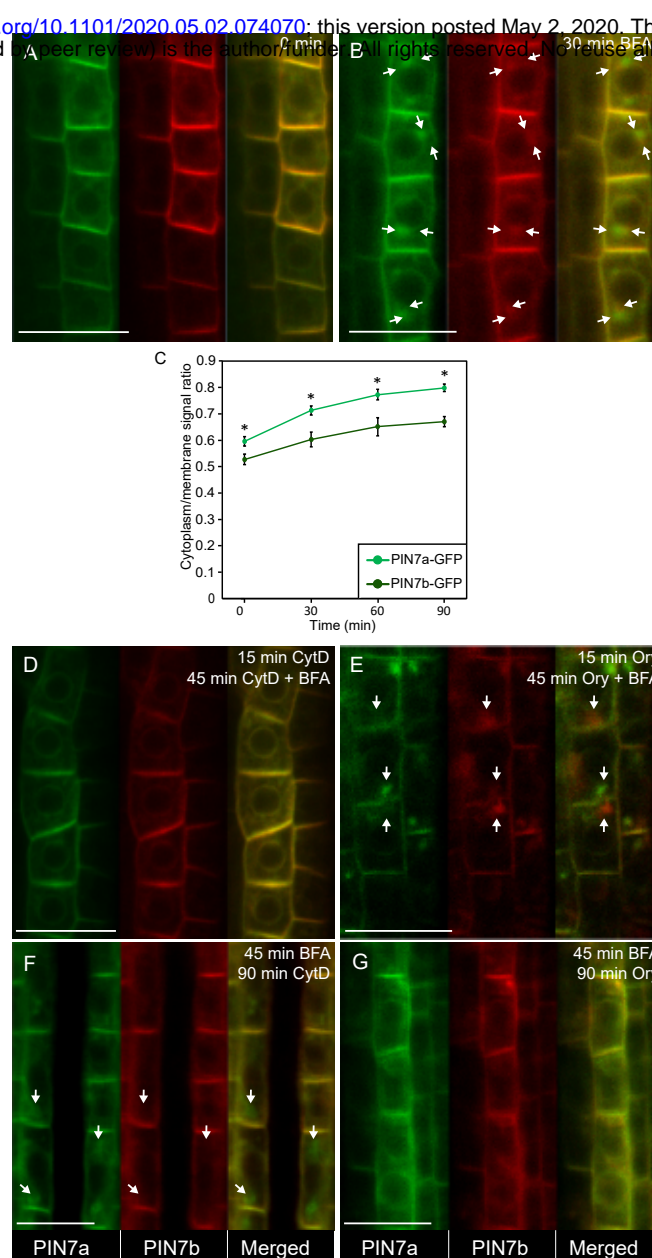
6

Figure 2. PIN7a-GFP and PIN7b-RFP cDNA-encoded proteins show similar cellular localization patterns but differ in response to brefeldin A (BFA) and the cytoskeletal drugs in the Arabidopsis primary root meristem.

(A) Subcellular localization and polarity of untreated PIN7a-GFP and PIN7b-RFP cDNA-encoded proteins in the primary root meristem cells.

(B) Both PIN7a-GFP and PIN7b-RFP aggregate in the intracellular compartments (BFA bodies) after 30 min of 50 μM BFA treatment, but do not fully co-localize (arrows).

(C) Temporal dynamics of BFA mediated aggregation of PIN7a-GFP and PIN7b-GFP inside cells. The values were determined as a ratio of fluorescence intensities between the cytoplasm and plasma membrane. (*P < 0.05 by ANOVA, n = 12). Data are means ± S. E.

(D) The fluorescence signal from PIN7a-GFP and PIN7b-RFP upon disruption of actin filaments with 20 μM cytochalasin D for 15 min followed by the addition of 50 μM BFA for another 45 min.

(E) PIN7a-GFP and PIN7b-RFP aggregation (arrows) upon disruption of microtubules with 20 μM oryzalin for 15 min, followed by the addition of 50 μM BFA for another 45 min.

(F) Effect of cytochalasin D on the PIN7a-GFP and PIN7b-RFP exit from the BFA bodies upon 45 min pre-treatment with 50 μM BFA and followed by wash-out with 20 μM cytochalasin D for another 90 min.

(G) Effect of oryzalin on the PIN7a-GFP and PIN7b-RFP exit from the BFA bodies upon 45 min pre-treatment with 50 μM BFA and followed by wash-out 20 μM oryzalin.

In (A, B and D-G), the signals of 3 cells in each of 5 root tips were analyzed (n = 15); bars, 10 μm.

See also Supplemental Figure 2.

156   oryzalin (Geldner et al., 2001). In the presence of cytochalasin D, PIN7a-GFP largely

157   persisted inside the BFA bodies, while the PIN7b-RFP signal was almost absent in these

158   aggregates (Figure 2F). We generally did not see any difference between both isoforms when

159   BFA was washed out with oryzalin (Figure 2G). These data thereby suggest that both PIN7

160   isoforms use vesicle trafficking pathways that are assisted by a common cytoskeletal scaffold.

161   These pathways differ in their dynamics and the endomembrane components involved and are

162   consistent with previous findings that individual PINs can utilize multiple PM delivery routes

163   (Boutté et al., 2006; Kleine-Vehn et al., 2008b).

164

165   **AS affects dynamics of PIN7 at the PM but not its ability to relocate in response to**

166   **tropic stimuli**

167   Complementary to the observations obtained by the pharmacological approach, we

168   tracked intracellular PIN7 dynamics under natural conditions. Auxin transporters of the PIN3

169   clade change their polar localization on the PM by the reaction to various environmental cues,

170   in particular by switching the light or gravity vectors (Friml et al., 2002; Rakusová et al.,

171   2011; Ding et al., 2011). PIN3 relocation in response to gravity in columella root cells is seen

172   in as little as 2 min, while the relocation of PIN7-GFP requires approximately 30 min to be

173   detected (Friml et al., 2002; Kleine-Vehn et al., 2010; Pernisova et al., 2016; Grones et al.,

174   2018). We examined plants harboring both *PIN7a-GFP* and *PIN7b-RFP* cDNAs under short

175   and long gravitropic stimuli. We did not find any difference in relocation dynamics between

176   both isoforms in these experiments (Supplemental Figures 3A-3D). We observed no

177   difference in the polarity change between PIN7a-GFP and PIN7b-RFP in hypocotyl

178   gravitropic (Rakusová et al., 2011; Rakusová et al., 2016) and phototropic (Ding et al., 2011)

179   bending assays (Supplemental Figures 3E-3I; due to limited transparency of hypocotyls, we

180   used lines expressing the cDNAs under strong endodermal *SCARECROW* (*SCR*) promoter

181   (Rakusová et al., 2011)). These data indicate that the different subcellular pathways driving

182   both PIN7a-GFP and PIN7b-RFP cargos are not connected with their ability to change

183   polarity in response to tropic stimuli.

184   Several studies employed the fluorescence recovery after photobleaching (FRAP)

185   analysis to investigate the dynamic turnover of various proteins, including PINs, on PM (Men

186   et al., 2008; Martinière et al., 2012; Langowski et al., 2016). We therefore bleached a region

187   of the PM signal in the root meristem of the *PIN7a-GFP* and *PIN7b-GFP* cDNA lines and

188   measured the FRAP in this area. Notably, PIN7a-GFP showed a slower recovery of

189   fluorescence than PIN7b-GFP (Figure 3A). The difference in the recovery speed and also in
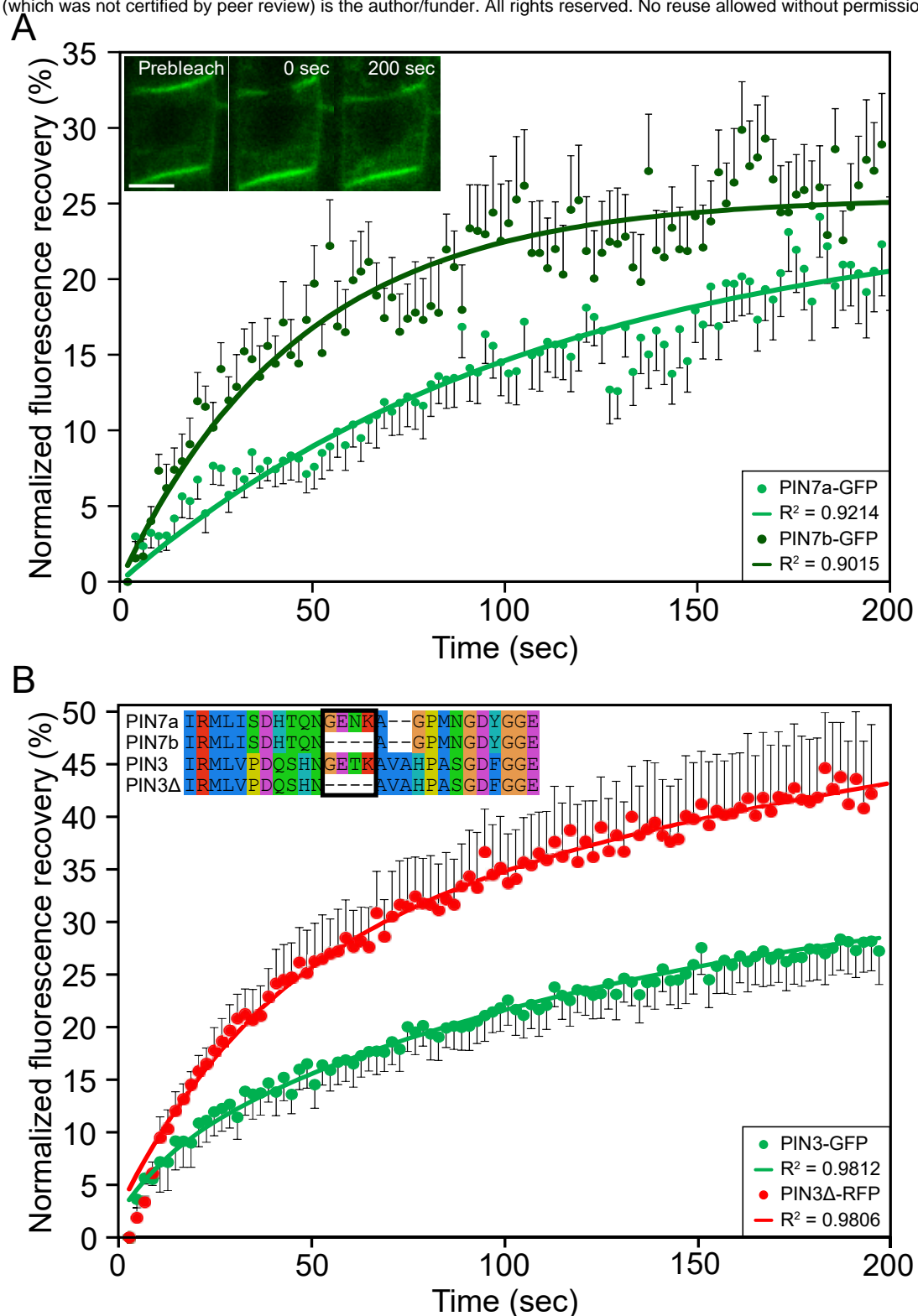
Figure 3. The cDNA encoded PIN7a and PIN7b isoforms tagged with fluorescent proteins show differential dynamics on the plasma membrane, as revealed by fluorescence recovery after photobleaching (FRAP).

(A) The PIN7a-GFP and PIN7b-GFP normalized FRAP, with single-phase exponential fitting curves. PIN7b-GFP shows different fluorescence recovery on the plasma membrane, compared to the longer PIN7a-GFP. The example image of the bleached region in cells is shown on the inset.

(B) The PIN3Δ-RFP and PIN3-GFP normalized FRAP, with single-phase exponential fitting curves. PIN3Δ-RFP, which lacks the 4 amino acid motif to mimic the properties of the PIN7b isoform, shows faster fluorescence recovery, in comparison to the control PIN3-GFP.
Bars, 5 μm. Data are means, error bars are ± S. E. At least 3 membranes in 5-6 root tips were analyzed in each experiment (n ≥ 20).

See also Supplemental Figures 3 and 4.

9

190 the overall mobile phase ratio was even more pronounced when we used lines expressing both

191 cDNAs under the stronger *SCR* promoter (Supplemental Figure 4A); the choice of GFP or

192 RFP tag did not markedly interfere with the fluorescence recovery (Supplemental Figure 4B).

193 To validate our observations further, we generated plants carrying a *PIN3::PIN3Δ-RFP*

194 cDNA construct, which lacks the GETK motif corresponding to the four amino acids absent

195 in PIN7b (Figures 1B and 3B). The PIN3Δ-RFP signal showed an incomplete co-localization

196 with the wild type PIN3-GFP variant in the BFA bodies (Supplemental Figures 4C and 4D),

197 and faster recovery on the PM, analogous to that observed for PIN7a and PIN7b (Figure 3B).

198 It therefore appears that the motif altered by AS of PIN7 is required for the regulation of

199 dynamics of individual isoforms within the PM.

200

201 **PIN7 splice isoforms are functionally different, based on the phenotype rescue tests**

202 To explore the role of the *PIN7* splice isoforms in plant development, we tested the

203 ability of their fluorescently tagged cDNAs to complement the phenotypes associated with the

204 *PIN7* locus. We initially selected the phototropic hypocotyl bending assay, which is highly

205 dependent on the activity of the PIN3 clade proteins (Friml et al., 2002; Willige et al., 2013).

206 We were unable to detect significant defects in the single *pin7-2* knockout (Friml et al., 2003)

207 itself, even at a detailed temporal resolution (Supplemental Figure 5A). As weak phenotypes

208 of the *pin7-2* loss of function mutants are the result of redundancy with other genes from the

209 *PIN3* clade (Friml et al., 2003; Blilou et al., 2005; Willige et al., 2013), we further employed a

210 triple *pin3-3 pin4-101 pin7-102* knock out (*pin347*) as a genetic background, which lacks the

211 phototropic response almost completely (Willige et al., 2013). Here, *PIN7a-GFP* cDNA was

212 able to rescue the phototropic bending, while the *PIN7b-RFP* cDNA did not show any effect,

213 regardless of whether the native (Figure 4A) or a strong endodermal *SCR* promoter

214 (Supplemental Figure 5B), was used. The choice of the tag does not appear to have any effect

215 in these assays, as evidenced by the lines where the fluorophore sequences have been

216 swapped (Figure 4B). Together, these data indicate that the motif changed by AS alters the

217 function of the PIN7 protein in *Arabidopsis*.

218 *PIN7a*, but not *PIN7b*, cDNA rescues the *pin347* phenotypes in the hypocotyl bending

219 test, and PIN3 clade auxin efflux carries have been implicated in numerous instances of

220 auxin-mediated development. We therefore tested whether in some them the role of the

221 particular isoform could be prevalent. These processes include: determining of root

222 protoxylem formation (Bishopp et al., 2011) (Figure 4C), lateral root density (Swarup et al.,

223 2008) (Figure 4D), vertical direction of the root growth (Friml et al., 2002; Kleine-Vehn et al.,
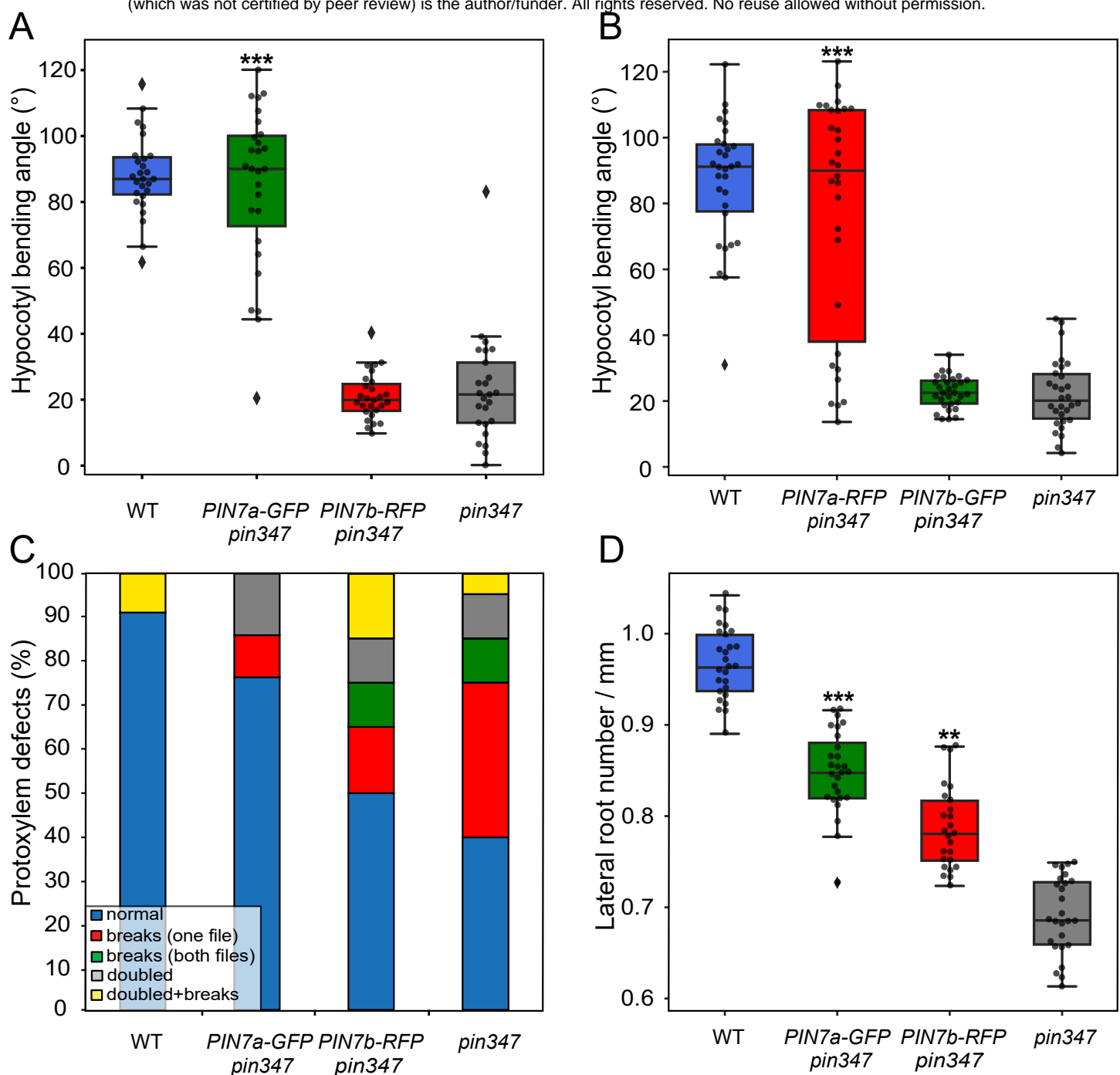
Figure 4. In contrast to PIN7b, the PIN7a cDNA under control of the natural PIN7 promoter complements phenotypes associated with the PIN7 locus.

(A) Phototropic bending of the etiolated pin347 seedlings carrying the PIN7a-GFP and PIN7b-RFP constructs.

(B) Phototropic bending of the etiolated pin347 seedlings carrying the PIN7a-RFP and PIN7b-GFP constructs.

(C and D) Quantification of the primary root protoxylem defects (C) and lateral root primordia (D) initiation of the pin347 seedlings harboring the PIN7a-RFP and PIN7b-GFP constructs.

On (A), (B) and (D), the middle line corresponds to median, the box corresponds to the 25% and 75% quartiles, the whiskers correspond to minima and maxima, dots represent single data points. The asterisks indicate significance between respective line and the pin347 mutant control (**$P < 0.01$, ***$P < 0.001$ by ANOVA). For each line in each experiment, at least 15 seedlings were analyzed (n ≥ 15).

See also Supplemental Figure 5.

11

224   2010; Pernisova et al., 2016) (Supplemental Figure 5C), lateral root orthogravitropism

225   (Rosquete et al., 2013) (Supplemental Figure 5D), gravity-induced hypocotyl bending

226   (Rakusová et al., 2011) (Supplemental Figure 5E), number of rosette branches after

227   decapitation (Bennett et al., 2016) (Supplemental Figure 5F) and the overall rosette size

228   (Bennett et al., 2016) (Supplemental Figure 5G). Similar to the results above, the *PIN7a-GFP*

229   cDNA usually almost completely rescued the tested phenotypes, while the contribution of

230   *PIN7b-RFP* was smaller or even undetectable. This suggests that the functional roles of both

231   isoforms are common, regardless of the phenotype observed.

232

233   **A fluorescent reporter for studying the *PIN7a* and *b* expression**

234   The levels of *PIN7* (and *PIN4*) AS transcripts seem to be at comparable levels in most

235   organs (Figure 1C and Supplemental Figure 1A). However, this may not describe the actual

236   situation at the resolution of individual cells. To address this, we designed a dual fluorescent

237   reporter, which allows for monitoring the activity of the AS of *PIN7 in planta* and *in situ*

238   (Figure 5A). Indeed, in the primary root or in the hypocotyl, we observed generally

239   overlapping expression of both isoforms without any obvious tissue preference (Figure 5B;

240   Supplemental Figure 6A). However, there were several instances in the vegetative tissue,

241   where the ratio of reporter signals appears to be uneven. These include early lateral root

242   primordia (Figure 5C), the mature pericycle adjacent to the phloem area (Supplemental Figure

243   6B), the stomatal lineage ground cells of the cotyledons (Supplemental Figure 6C), and the

244   concave side of opening apical hook (Figures 5D), where the PIN7b-RFP signal prevailed

245   over that of PIN7a-GFP. In general, these data corroborate the presence of both isoforms in

246   most cells and suggest that they may function in a coordinated manner.

247

248   **The combined activity of both PIN7a and PIN7b is required for apical hook formation**

249   **and tropic responses**

250   The occasional exaggerated response of the *pin347* mutants containing the *PIN7a-*

251   *GFP* transgene (Supplemental Figure 5E) prompted us to re-design phenotypic tests and adapt

252   our experimental methodology to carefully record the temporal dynamics of the processes

253   linked with the PIN3 clade function. We turned to apical hook development where the time

254   scale measurements of the PIN-mediated development have been well established (Zadnikova

255   et al., 2010). We also analyzed *pin4-101 pin7-102* (*pin34*) mutants and a newly generated

256   *pin347* line that carried a combination of both *PIN7* cDNA constructs. Similar to gravi- and

257   phototropic experiments, the *PIN7b-RFP* cDNA generally did not complement the severe
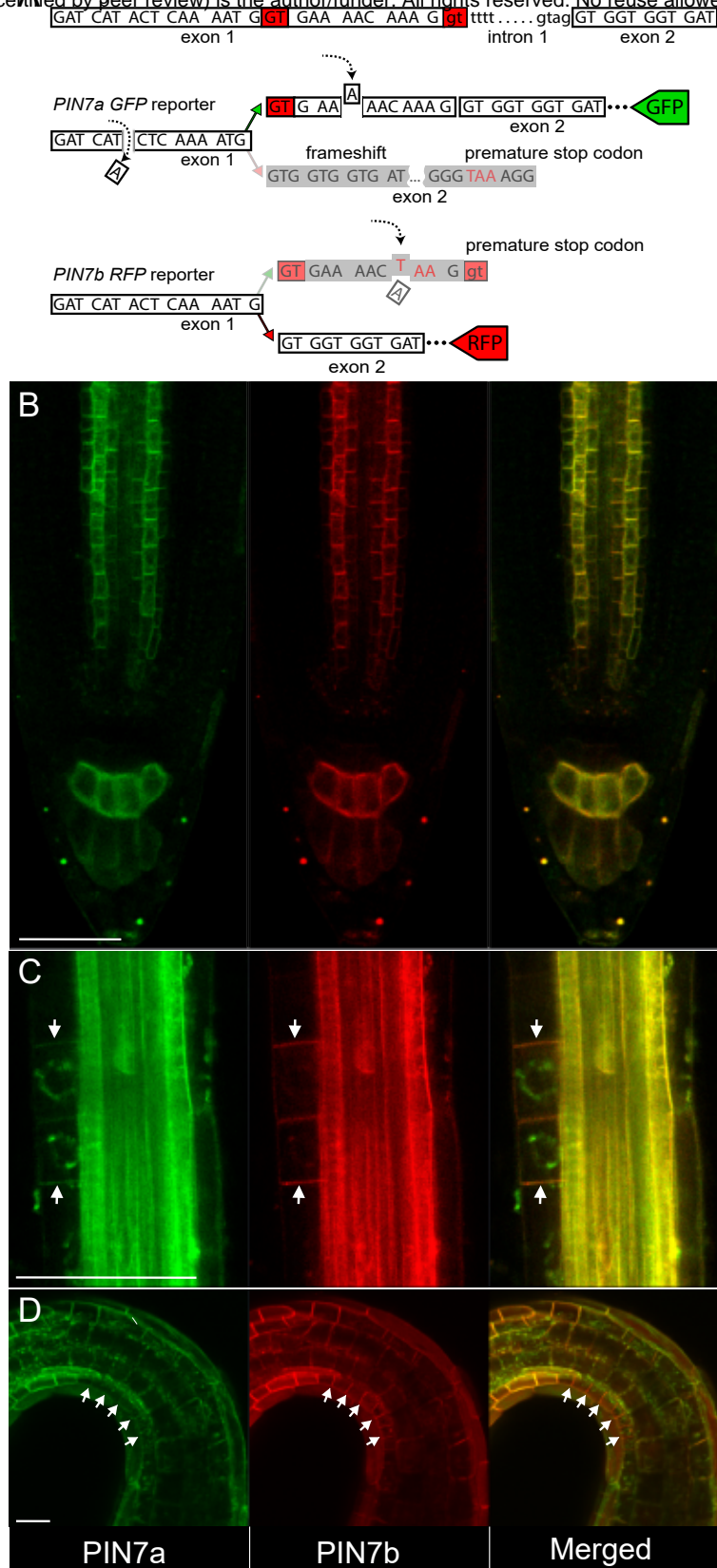
12

Figure 5. Reporter-based expression analysis of PIN7a and PIN7b isoforms across tissues.

(A) A scheme of the PIN7 splicing reporter. The reporter consists of two constructs: the PIN7a-GFP part contains two point mutations (marked with dashed arrows) and leads to the frameshift and its subsequent restoration when the PIN7a transcript is solely produced. PIN7b-RFP reporter carries a premature stop codon inside the protruding PIN7a region (dashed arrow below).

(B) PIN7a-GFP and PIN7b-RFP expression overlap in the root tip.

(C and D) PIN7b-RFP expression (arrows) PIN7a-GFP in the early lateral root primordia (C) and in the epidermis on the concave side of apical hook (D). The green signal in the perinuclear region of the lateral root primordia is an autofluorescence artifact.
For each tissue, at least 10 plants were analyzed (n ≥ 10). Bars, 50 μm.

See also Supplemental Figure 6.

13

258   *pin347* phenotype. Expression of the *PIN7a-GFP* cDNA in *pin347* indeed led to partial rescue

259   of the apical hook formation defects, even surpassing the values observed for *pin34*.

260   Surprisingly, the simultaneous expression of both *PIN7a-GFP* and *PIN7b-RFP* suppressed the

261   dominant effects conferred by the *PIN7a-GFP* cDNA alone and phenocopied the *pin34*

262   mutant (Figure 6A; this effect was not caused by suppressing the expression of PIN7a-GFP by

263   the other transgene, Supplemental Figure 6D). This strongly suggests that both isoforms act in

264   a mutually opposing manner to modulate the processes of apical hook development.

265   Apical hook formation is a complex process that involves several bending steps

266   (Zadnikova et al., 2010), and the splicing reporter suggests a slightly different expression

267   pattern of *PIN7a* and *b* isoforms during apical hook development (Figure 5D). The hypocotyl

268   phototropic and gravity response includes only a single bending (Rakusová et al., 2011;

269   Rakusová et al., 2016), and the expression of the reporter appears to be uniform in the

270   respective tissue (Supplemental Figure 6A). Tracking dynamic bending of hypocotyls can

271   thus provide a hint to whether one can account for the antagonistic behavior of both isoforms

272   to differential expression or to their different dynamics during subcellular trafficking or at the

273   PM. Similar to apical hook development (Figure 6A), introducing the *PIN7b-RFP* cDNA did

274   not have any effect on the *pin347* phenotype, while the expression of *PIN7a-GFP* lead to

275   more rapid bending than that observed for the *pin34* mutant. Finally, the presence of both

276   *PIN7a-GFP* and *PIN7b-RFP* cDNAs in *pin347* was reminiscent of the *pin34* phenotype in

277   both phototropic and gravity assays (Figures 6B and 6C). We therefore conclude that the

278   shared activity of both PIN7 isoforms, likely conferred by their different trafficking or PM

279   retention properties, but probably not by their differential expression, is required for proper

280   apical hook formation and auxin-mediated tropic responses.

281

282   **DISCUSSION**

283   In this study, we show that AS diversifies the portfolio of PIN proteins present in

284   *Arabidopsis thaliana*. At the cellular level, AS does not alter the ability of the PIN7 proteins

285   to transport auxin *per se* or their overall subcellular localization, but it changes their dynamics

286   on the PM. In general, AS modifies protein properties variably. It can affect protein

287   subcellular localization, ligand binding affinity, enzymatic or transporting activities, protein

288   stability or the presence of covalent post-translational modifications (Stamm et al., 2005;

289   Kelemen et al., 2013). Different covalent modifications alter the subcellular trafficking of

290   most PINs. Phosphorylation sites on serine, threonine or tyrosine residues of various PINs

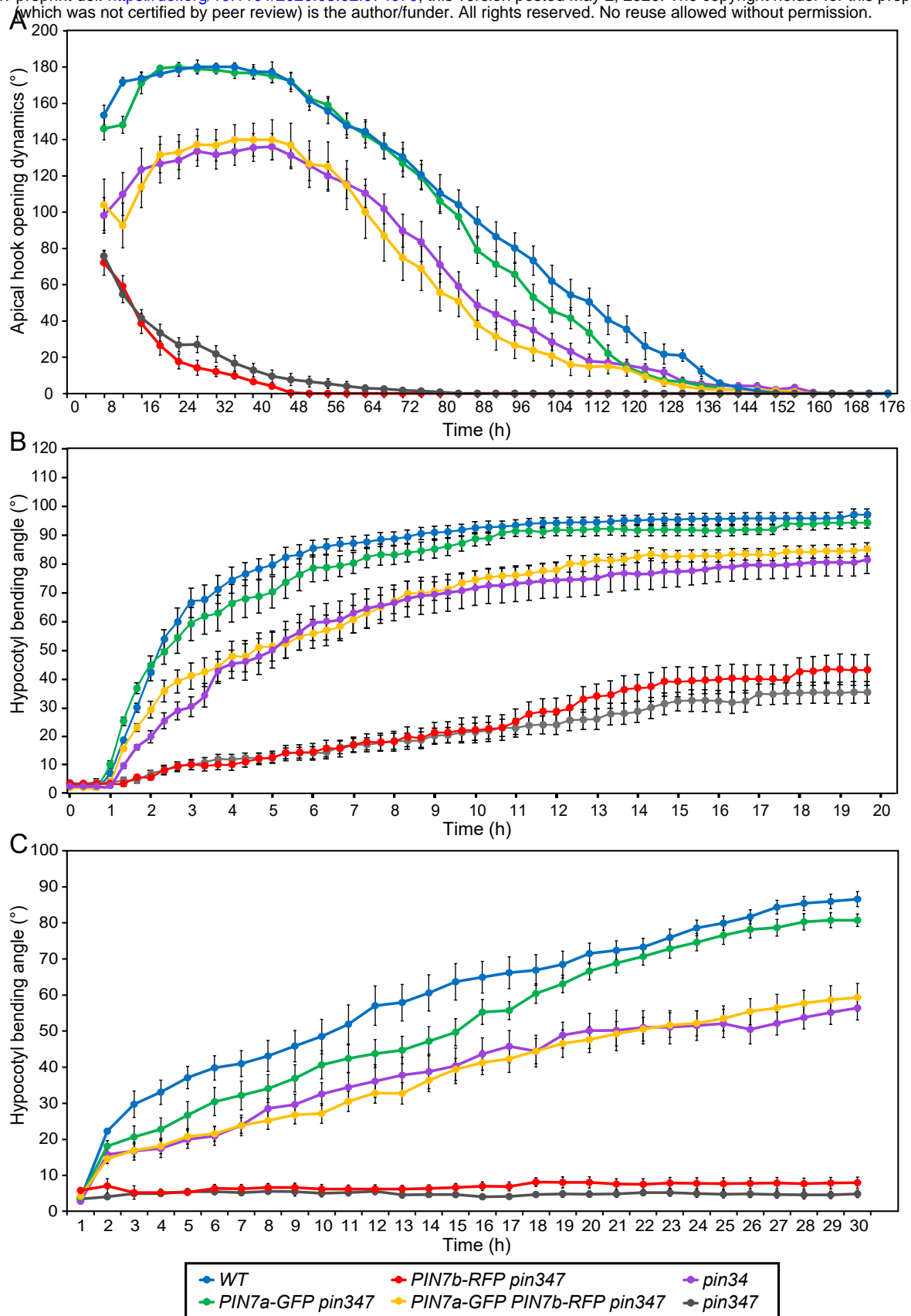291   have been identified; their phosphorylation status also changes PIN-mediated tropic responses

14

Figure 6. The simultaneous presence of PIN7a-GFP and PIN7b-RFP cDNA constructs in pin347 phenocopies the pin34 knock out mutant during apical hook opening and hypocotyl gravitropic bending.

(A-C) Temporal dynamics of etiolated pin347 seedlings carrying the PIN7a-GFP and PIN7b-RFP transgenes examined (A) during apical hook development, (B) hypocotyl phototropic and (C) gravitropic bending.

Data are means ± S. E. For each data point, the values obtained from 15 vertically grown seedlings were assessed (n = 15).

15

292   (Rademacher and Offringa, 2012; Barbosa et al., 2018; Zwiewka et al., 2019). Also PIN

293   ubiquitination (on lysines) and controlled proteolytic degradation act in auxin-mediated

294   processes (Leitner et al., 2012). However, none of the candidate residues required for these

295   modifications is present in the vicinity of the amino acid motif changed by AS. This region,

296   present inside the PIN long hydrophilic loop shows low amino acid conservation and it is

297   perhaps intrinsically disordered (Figure 1C) (Zwiewka et al., 2019). One can therefore

298   speculate whether it may change, perhaps by its length, the ability to assemble internal PIN

299   domains within the long hydrophilic group (Buljan et al., 2013) and modulate their interaction

300   affinity with other factors required for the entry and presence in secretory pathways and/or for

301   PIN7 dynamics at the PM.

302   We also present genetic evidence that the mutual activity of PIN7a and PIN7b is

303   operational during apical hook formation and tropic responses. We also tested major

304   functional aspects linked with the cellular activity of PIN7 that might be responsible for the

305   observed phenotypes (Adamowski and Friml, 2015). We found the differences between

306   PIN7a and PIN7b at the level of the PM recycling pathways and the stability on the plasma

307   membrane. It was previously demonstrated that the dynamics of PINs on the PM is controlled

308   in principle by two factors: by lateral diffusion in earlier phases and by dynamic recycling

309   from the secretory pathways in longer timelines (Kleine-Vehn et al., 2008a; Kleine-Vehn et

310   al., 2011; Langowski et al., 2016). As the effect of secretion or recycling has been evidenced

311   to be minor within 10 min after photobleaching (Kleine-Vehn et al., 2011; Langowski et al.,

312   2016), it seems that lateral diffusion significantly participates on the differential behavior of

313   PIN7a and PIN7b. In accordance with previous findings (Kleine-Vehn et al., 2011; Feraru et

314   al., 2011; Langowski et al., 2016), slower PIN7a FRAP rates suggest that PIN7 properly

315   functions when only associated with a larger complex or inside stable membrane clusters.

316   According to the earlier published model (Langowski et al., 2016), it therefore seems that

317   PIN7b probably antagonizes PIN7a action by impeding the polar auxin flow provided by

318   PIN7a in these membrane domains (Supplemental Figure 6E).

319   The mutually antagonistic interaction between two splice isoforms (or a similar

320   coordinated mechanism) has generally been already proposed in *Arabidopsis* (Szakonyi and

321   Duque, 2018). The seed dormancy regulator *DELAY OF GERMINATION 1* (*DOG1*) is

322   processed into five mRNAs. Only the expression of two or more DOG1 cDNAs under the

323   native promoter rescues the *dog1* phenotype by synergistic stabilization of the protein by its

324   multimerization (Nakabayashi et al., 2015). The transcription factor HYH (HY5

325   HOMOLOG) possesses an isoform, which lacks a domain required for proteasomal

16

326   degradation, which leads to its increased stability and probably works as a semi-dominant

327   splice variant (Sibout et al., 2006; Szakonyi and Duque, 2018). The example of AS of PIN7 is

328   thus one of the first instances in plants where the mutually antagonistic effects of two splice

329   isoforms are observed on a single gene.

330

331   **EXPERIMENTAL PROCEDURES**

332   **Plant material and plant growth conditions**

333   All plant material, except tobacco cell cultures, was in the *Arabidopsis thaliana* (L.)

334   Heynh., Col-0 ecotype. These mutant and transgenic lines were described previously:

335   *PIN3::PIN3-GFP* (Zadnikova et al., 2010)*, PIN4::PIN4-GFP*, *PIN7::PIN7-GFP* (Blilou et

336   al., 2005), *pin3-3 pin4-101 pin7-102* (*pin347*), *pin3-3 pin4-101* (*pin34*) (Willige et al., 2013)*,

337   *pin7-2* (Friml et al., 2003)*.

338   For the *in vitro* cultivation, the seeds were surface-sterilized for 5 h with chlorine gas,

339   plated on 0.5× Murashige & Skoog medium with 1 % sucrose, and then stratified for 2 d at

340   4°C in darkness. Unless indicated otherwise, the seedlings were grown on vertically oriented

341   plates for 4-6 days under 16 h : 8 h photoperiod, 22 : 18°C, light : dark.

342   The following chemicals were used for treatments: brefeldin A (BFA), cytochalasin D

343   (CytD), oryzalin (Ory), β-estradiol, 2,4-dichlorophenoxyacetic acid (2,4-D), all from Sigma

344   (Sigma-Aldrich, St. Louis, MO, USA). Radioactively labeled auxin accumulation assays were

345   performed with [^{3}H]NAA (naphthalene-1-acetic acid; 20 Ci.mmol^{-1}; American Radiolabeled

346   Chemicals, St. Louis, MO, USA).

347

348   **DNA manipulations and transgenic work**

349   The genomic *PIN7::PIN7-RFP* construct was made by replacing the GFP coding

350   sequence in the original *PIN7::PIN7-GFP* construct (Blilou et al., 2005). For creating the

351   *PIN7(4)::PIN7(4)a-GFP* and *PIN7(4)::PIN7(4)b-RFP* cDNA constructs, the respective

352   cDNAs were cloned into the pDONR221 P5-P2 entry vector (Invitrogen, Life Technologies,

353   Carlsbad, CA., USA) by the Gateway BP reaction (Invitrogen). The *Xba*I restriction site was

354   introduced at the 1350 bp (for *PIN7*) or 1341 bp (for *PIN4*) position of the cDNA coding

355   region for placing the fluorophore tag sequence. In parallel, the *PIN7* (or *PIN4*) promoters

356   were inserted into the pH7WG Gateway vector (Department of Plant Systems Biology, Ghent

357   University, Belgium; Karimi et al., 2002) by the Gibson Assembly kit (New England Biolabs,

358   Ipswich, MA, USA). The tagged *PIN7* and *PIN4* cDNA entry clones were then recombined

359   with the modified pH7WG destination vector by the Gateway LR reaction (Invitrogen). For

360   the cloning of the *PIN7* splicing dual fluorescent reporter, the entry vectors carrying the

361   genomic sequence of *PIN7-GFP* and *PIN7-RFP* (Adamowski and Friml, 2015), respectively,

362   were modified by inverse PCR. The resulting constructs were then recombined by the

363   Gateway LR reaction with the *PIN7* promoter containing the pH7WG destination vector. The

364   *SCR::PIN7a-GFP* and *SCR::PIN7b-RFP* constructs were obtained by recombination of the

365   *SCR* promoter in pDONR221 P1-P5r and *PIN7* cDNA entry clones with the pH7WG

366   destination vector by the Multisite Gateway LR reaction. *PIN3Δ-RFP* cDNA was custom

367   synthesized (Gen9, Ginkgo Bioworks, Boston, MA, USA), cloned into pDONR221 P5-P2

368   vector and together with the *PIN3* promoter pDONR221 P1-P5r construct recombined into the

369   pH7WG vector with Multisite Gateway. The validated binary constructs were transformed

370   into *Arabidopsis* by floral dipping. For making the estradiol-inducible *G10-*

371   *90::XVE>>AtPIN7(4)a-GFP*, and *G10-90::XVE>>AtPIN7(4)b-GFP* constructs, tagged *PIN7*

372   or *PIN4* cDNA entry clones were recombined with the pMDC7 destination vector (Curtis and

373   Grossniklaus, 2003) by the Gateway LR reaction. Unless stated otherwise, the constructs

374   present in the study were cloned under their natural *PIN4* or *PIN7* promoter. Primers used in

375   this work are listed in Supplemental Table 1.

376   For the generation of the stable transgenic lines carrying the cDNA constructs, at least

377   eight independent descendant populations of primary transformants were preselected for the

378   presence of the fluorescent signal. The functional validity of the cDNA constructs was

379   verified in the phototropic bending test, where all candidate lines matched the presented

380   results. Selected lines were used for further phenotypic analysis.

381

Plant phenotype analysis

383   The dynamic seedling development was tracked in the custom made dynamic

384   morphogenesis observation chamber equipped with blue and white LED unilateral light

385   sources, infra-red LED back light and a camera for imaging in the infra-red spectra, controlled

386   by the Raspberry Pi3B microcomputer (Raspberry Pi foundation, Cambridge, UK). For the

387   hypocotyl bending assays, the plated seeds were first illuminated for 6 h with white light. The

388   plates were then transferred to the observation chamber for 3-4 d. For the hypocotyl

389   phototropic bending experiments (Friml et al., 2002), the dark-grown seedlings were

390   afterward illuminated for 20 h with unilateral white light and imaged every 20 minutes. For

391   hypocotyl gravitropic bending experiments (Rakusová et al., 2011), the dark-grown seedlings

392   were rotated by 90° clockwise and imaged for 30 h every 60 min. For tracking apical hook

393   development, the seeds were first illuminated for 6 h with white light. They were then

394   transferred to the observation chamber and their development recorded every 4 h for a total

395   150 - 200 h in infrared spectra. Germination time was set as time 0, when first traces of the

396   main root were observed, individually for each seedling analyzed. Apical hook was

397   determined as an angle between the immobile (non-bending) part of hypocotyl and the distal

398   edge of cotyledons (Zadnikova et al., 2010), using the ImageJ software (Rueden et al., 2017).

399   At least 15 seedlings were analyzed for each line. Each experiment was done at least three

400   times.

401   For protoxylem defects analysis, 5-d old light-grown seedlings were cleared and

402   analyzed as described previously (Bishopp et al., 2011). For examining lateral root density, 8-

403   d old light-grown seedlings were cleared and observed with a DIC microscope (Dubrovsky et

404   al., 2009). Lateral root density was calculated by dividing the total number of lateral roots and

405   lateral root primordia to the length of the main root as described (Dubrovsky et al., 2009).

406   Vertical Growth Index (VGI), defined as a ratio between main root ordinate and main root

407   length, was quantified on 5-d old seedlings as published previously (Grabov et al., 2005). For

408   measuring the Gravitropic Set-point Angle (GSA), plates with 14-d old light-grown seedlings

409   were scanned and the angles between the vertical axis and five innermost 0.5 mm parts of

410   lateral root were determined as described previously (Roychoudhry et al., 2017). In all cases,

411   12-20 seedlings were analyzed for each line. Each experiment was done at least three times.

412   For decapitation experiments, 4-week short-day grown plants were moved into long-

413   day conditions to induce flowering. After the primary bolt reached 10-15 cm, the plant was

414   decapitated. The number of rosette branches was recorded at 7, 10 and 14-d after decapitation

415   (Greb et al., 2003; Waldie and Leyser, 2018). Rosette size was inspected in 18-d light-grown

416   plants prior to documenting. 10 plants were analyzed for each line, the experiment was done

417   three times.

418

419   **Microscopy**

420   Bright-field microscopy (differential interference contrast, DIC) was conducted on the

421   Olympus BX61 instrument (Olympus, Shinjuku, Tokyo, Japan) equipped with a DP50 camera

422   (Olympus). Routine confocal microscopy was performed on inverted Zeiss Axio Observer.Z1

423   containing the standard confocal LSM880 and Airyscan modules with 20x/0.8 DIC M27 air,

424   40x/1.2 W Kor FCS M27 air and 63x/1.40 Oil DIC M27 objectives (Carl Zeiss AG, Jena,

425   Germany). Gravity-induced polarity change experiments were carried out on Zeiss Axio

426   Observer.Z1 with vertically oriented sample position and the 40x/0.75 glycerol objective.

19

427   To observe the light-induced polarity change of PIN7a-GFP and PIN7b-RFP, 4-d

428   dark-grown seedlings were irradiated for 4 h with unilateral white light and then imaged with

429   Zeiss Axio Observer.Z1 LSM880 with a vertically oriented sample position, as described

430   (Willige et al., 2013). For analyzing gravity-induced polarity change, 4-d dark-grown

431   seedlings were reoriented by 90° clockwise and imaged 6 and 24 h after rotation, as described

432   (Rakusová et al., 2011).

433   For BFA treatments, 5-d light-grown seedlings were transferred to liquid 0.5× MS

434   media containing 50 μM BFA. The membrane/cytosol ratio was determined with ImageJ, it

435   was defined as the mean membrane signal intensity divided by the mean fluorescence in the

436   cytosol. For cytoskeleton depolymerizing drug treatments (Geldner et al., 2001), 5-d light-

437   grown seedlings were transferred to liquid 0.5× MS media supplemented with 20 μM of

438   cytochalasin D or 20 μM oryzalin. The co-treatments were done by the direct addition of

439   BFA. For the BFA removal, prior to the addition of the cytoskeleton depolymerizing

440   compounds, seedlings were twice washed out with fresh media and then transferred to that

441   supplemented with the respective cytoskeleton-depolymerizing drug.

442

443   **Fluorescent recovery after photobleaching (FRAP)**

444   For the FRAP experiments, Zeiss Axio Observer.Z1 equipped with the LSM880

445   confocal and Airyscan modules and the 40x/1.2 W Kor FCS M27 air objective was used. A

446   rectangular region of interest (ROI) of 40 x 20 pixels was selected on the basal or apical PM

447   of cells inside the vascular cylinder in the primary root meristematic area of 5-d light-growth

448   seedlings. ROI was bleached with the maximum 488 nm laser intensity and fluorescence

449   recovery was documented every 1 or 2 sec for a total 200 sec. Recovery time lapses were

450   analyzed with ImageJ. The Slices Alignment plugin (Tseng et al., 2012) for ImageJ was used

451   for the elimination of cell movement caused by root growth. In parallel, another rectangular

452   ROI (100 x 20 pixels) on the non-bleached cell was selected as a reference. To compensate

453   for the fluorophore bleaching during the recovery period, the data were normalized using

454   equation (Laňková et al., 2016)

455
$$In \ = \frac{\left(\frac{It}{It_{ref}}\right) - \left(\frac{Imin}{Imin_{ref}}\right)}{\left(\frac{Imax}{Imax_{ref}}\right) - \left(\frac{Imin}{Imin_{ref}}\right)},$$

456   where *In* is normalized fluorescence intensity, *It* is the intensity at the specific time point,

457   *Imax* is the intensity after the initial bleaching, *Imax* is the intensity before initial bleaching.

458   *It_{ref}, Imax_{ref}* and *Imin_{ref}* represent the same values for the reference ROI. At least 3 membranes

459   in 4-5 root tips were analyzed in each experiment. Single-phase exponential fitting was

460   applied to the normalized FRAP data (SigmaPlot, Systat Software, Chicago, ILL, US) as

461   described (Sprague and McNally, 2005; Laňková et al., 2016). Recovery half-time is defined

462   as a time required for the fluorescence recovery to reach half of the steady-state fluorescence

463   intensity (Soumpasis, 1983; Sprague and McNally, 2005).

464

465   **Tobacco cell lines and auxin accumulation assays**

466   Tobacco cell line BY-2 (*Nicotiana tabacum* L. cv. Bright Yellow 2) was cultivated as

467   described (Müller et al., 2019). BY-2 cells were transformed with the pMDC7 constructs by

468   co-cultivation with *Agrobacterium tumefaciens* strain GV2260 as earlier described (Petrasek

469   et al., 2006; Müller et al., 2019). The transgene expression was maintained by cultivation on

470   media supplemented with 40 μg.ml^{-1} hygromycin (Roche) and 100 μg.ml^{-1} cefotaxime

471   (Sigma). Accumulation assays of radioactively labeled auxin were performed as previously

472   published (Delbarre et al., 1996; Petrasek et al., 2006) with cells cultured for 2 days in β-

473   estradiol or DMSO mock treatments. Presented results are from 3 biological replicates for

474   each representative *PIN7a* and *PIN7b* line and were confirmed for each on two other

475   independent genotypes. Independent β-estradiol inductions were done within 3-9 months after

476   the establishment of the cell suspension on lines, which showed comparable levels of the

477   expressed PIN7-GFP signal.

478

479   **Statistics and sequence analysis**

480   For two groups mean comparison, Student's *t*-test was applied. Statistical analysis of

481   multiple groups was performed by one-way ANOVA with subsequent Tukey HSD post-hoc

482   test. All statistical tests, including normality tests, were performed in R-studio IDE (R-studio,

483   Boston, MA, USA). In the box plots, the whisker length was defined as $Q \pm 1.5 \times$ IQR, where

484   Q is the corresponding quartile and IQR is the interquartile range. For creating the multiple

485   sequence alignments, the protein sequences were aligned using the Clustal Omega algorithm

486   (Sievers et al., 2011) and graphically outlined by Mega-X, using default ClustalX color code

487   (Kumar et al., 2018).

488
489   **ACKNOWLEDGMENT**

499

500   **AUTHOR CONTRIBUTIONS**

501   I. K., M. H., R. F., Z. V., D. R., and J. P. conducted experiments. J. H. enabled making

502   part of this project in his laboratory. S. S. and J. F. provided unpublished material. I. K., J. P.,

503   T. B. J., M. J. F., J. F., J. P., and K. R. conceived the research and designed experiments. K.

504   R. and I. K. wrote the manuscript. All authors read and commented on the final version of the

505   manuscript.

506

507   **DECLARATION OF INTERESTS**

508   The authors declare no competing interests.

509

510   **REFERENCES**

511   **Adamowski, M., and Friml, J.** (2015). PIN-Dependent Auxin Transport: Action, Regulation,
512   and Evolution. *Plant Cell* **27**:20–32.

513   **Barbosa, I. C. R., Hammes, U. Z., and Schwechheimer, C.** (2018). Activation and Polarity
514   Control of PIN-FORMED Auxin Transporters by Phosphorylation. *Trends in Plant*
515   *Science* **23**:523–538.

516   **Bazin, J., Romero, N., Rigo, R., Charon, C., Blein, T., Ariel, F., and Crespi, M.** (2018).
517   Nuclear Speckle RNA Binding Proteins Remodel Alternative Splicing and the Non-
518   coding Arabidopsis Transcriptome to Regulate a Cross-Talk Between Auxin and
519   Immune Responses. *Front Plant Sci* **9**:1209.

520   **Bennett, T., Brockington, S. F., Rothfels, C., Graham, S. W., Stevenson, D., Kutchan, T.,**
521   **Rolf, M., Thomas, P., Wong, G. K.-S., Leyser, O., et al.** (2014). Paralogous
522   Radiations of PIN Proteins with Multiple Origins of Noncanonical PIN Structure. *Mol*
523   *Biol Evol* **31**:2042–2060.

524   **Bennett, T., Hines, G., Rongen, M. van, Waldie, T., Sawchuk, M. G., Scarpella, E.,**
525   **Ljung, K., and Leyser, O.** (2016). Connective Auxin Transport in the Shoot
526   Facilitates Communication between Shoot Apices. *PLOS Biology* **14**:e1002446.

527   **Bishopp, A., Help, H., El-Showk, S., Weijers, D., Scheres, B., Friml, J., Benková, E.,**
528   **Mähönen, A. P., and Helariutta, Y.** (2011). A mutually inhibitory interaction

529 between auxin and cytokinin specifies vascular pattern in roots. *Curr. Biol.* **21**:917–
530   926.

531 **Blencowe, B. J.** (2017). The Relationship between Alternative Splicing and Proteomic
532   Complexity. *Trends in Biochemical Sciences* **42**:407–408.

533 **Blilou, I., Xu, J., Wildwater, M., Willemsen, V., Paponov, I., Friml, J., Heidstra, R.,**
534   **Aida, M., Palme, K., and Scheres, B.** (2005). The PIN auxin efflux facilitator
535   network controls growth and patterning in Arabidopsis roots. *Nature* **433**:39–44.

536 **Boutté, Y., Crosnier, M.-T., Carraro, N., Traas, J., and Satiat-Jeunemaitre, B.** (2006).
537   The plasma membrane recycling pathway and cell polarity in plants: studies on PIN
538   proteins. *J. Cell. Sci.* **119**:1255–1265.

539 **Buljan, M., Chalancon, G., Dunker, A. K., Bateman, A., Balaji, S., Fuxreiter, M., and**
540   **Babu, M. M.** (2013). Alternative splicing of intrinsically disordered regions and
541   rewiring of protein interactions. *Current Opinion in Structural Biology* **23**:443–450.

542 **Casson, S. A., Topping, J. F., and Lindsey, K.** (2009). MERISTEM-DEFECTIVE, an RS
543   domain protein, is required for the correct meristem patterning and function in
544   Arabidopsis. *The Plant Journal* **57**:857–869.

545 **Cheng, C.-Y., Krishnakumar, V., Chan, A. P., Thibaud‐Nissen, F., Schobel, S., and**
546   **Town, C. D.** (2017). Araport11: a complete reannotation of the Arabidopsis thaliana
547   reference genome. *The Plant Journal* **89**:789–804.

548 **Curtis, M. D., and Grossniklaus, U.** (2003). A gateway cloning vector set for high-
549   throughput functional analysis of genes in planta. *Plant Physiol.* **133**:462–469.

550 **Darracq, A., and Adams, K. L.** (2013). Features of evolutionarily conserved alternative
551   splicing events between Brassica and Arabidopsis. *New Phytologist* **199**:252–263.

552 **Delbarre, A., Muller, P., Imhoff, V., and Guern, J.** (1996). Comparison of mechanisms
553   controlling uptake and accumulation of 2,4-dichlorophenoxy acetic acid, naphthalene-
554   1-acetic acid, and indole-3-acetic acid in suspension-cultured tobacco cells. *Planta*
555   **198**:532–541.

556 **Ding, Z., Galván-Ampudia, C. S., Demarsy, E., Łangowski, Ł., Kleine-Vehn, J., Fan, Y.,**
557   **Morita, M. T., Tasaka, M., Fankhauser, C., Offringa, R., et al.** (2011). Light-
558   mediated polarization of the PIN3 auxin transporter for the phototropic response in
559   Arabidopsis. *Nat Cell Biol* **13**:447–452.

560 **Dubrovsky, J. G., Soukup, A., Napsucialy-Mendivil, S., Jeknic, Z., and Ivanchenko, M.**
561   **G.** (2009). The lateral root initiation index: an integrative measure of primordium
562   formation. *Ann. Bot.* **103**:807–817.

563 **Feraru, E., Feraru, M. I., Kleine-Vehn, J., Martinière, A., Mouille, G., Vanneste, S.,**
564   **Vernhettes, S., Runions, J., and Friml, J.** (2011). PIN Polarity Maintenance by the
565   Cell Wall in Arabidopsis. *Current Biology* **21**:338–343.

566 **Friml, J., Wiśniewska, J., Benková, E., Mendgen, K., and Palme, K.** (2002). Lateral
567   relocation of auxin efflux regulator PIN3 mediates tropism in Arabidopsis. *Nature*
568   **415**:806–809.

569 **Friml, J., Vieten, A., Sauer, M., Weijers, D., Schwarz, H., Hamann, T., Offringa, R., and**
570   **Jürgens, G.** (2003). Efflux-dependent auxin gradients establish the apical-basal axis
571   of Arabidopsis. *Nature* **426**:147–153.

572 **Ganguly, A., Park, M., Kesawat, M. S., and Cho, H.-T.** (2014). Functional Analysis of the
573   Hydrophilic Loop in Intracellular Trafficking of Arabidopsis PIN-FORMED Proteins.
574   *Plant Cell* **26**:1570–1585.

575 **Geldner, N., Friml, J., Stierhof, Y. D., Jürgens, G., and Palme, K.** (2001). Auxin transport
576   inhibitors block PIN1 cycling and vesicle trafficking. *Nature* **413**:425–428.

577 **Ghelli, R., Brunetti, P., Napoli, N., Paolis, A. D., Cecchetti, V., Tsuge, T., Serino, G.,**
578   **Matsui, M., Mele, G., Rinaldi, G., et al.** (2018). A Newly Identified Flower-Specific
579   Splice Variant of AUXIN RESPONSE FACTOR8 Regulates Stamen Elongation and
580   Endothecium Lignification in Arabidopsis. *Plant Cell* **30**:620–637.

581 **Glanc, M., Fendrych, M., and Friml, J.** (2018). Mechanistic framework for cell-intrinsic re-
582   establishment of PIN2 polarity after cell division. *Nat. Plants* **4**:1082–1088.

583 **Grabov, A., Ashley, M. K., Rigas, S., Hatzopoulos, P., Dolan, L., and Vicente-Agullo, F.**
584   (2005). Morphometric analysis of root shape. *New Phytol.* **165**:641–651.

585 **Greb, T., Clarenz, O., Schafer, E., Muller, D., Herrero, R., Schmitz, G., and Theres, K.**
586   (2003). Molecular analysis of the LATERAL SUPPRESSOR gene in Arabidopsis
587   reveals a conserved control mechanism for axillary meristem formation. *Genes Dev.*
588   **17**:1175–1187.

589 **Grones, P., Abas, M., Hajný, J., Jones, A., Waidmann, S., Kleine-Vehn, J., and Friml, J.**
590   (2018). PID/WAG-mediated phosphorylation of the Arabidopsis PIN3 auxin
591   transporter mediates polarity switches during gravitropism. *Sci Rep* **8**:10279.

592 **Hrtyan, M., Šliková, E., Hejátko, J., and Růžička, K.** (2015). RNA processing in auxin and
593   cytokinin pathways. *J. Exp. Bot.* **66**:4897–4912.

594 **Kalyna, M., Lopato, S., and Barta, A.** (2003). Ectopic Expression of atRSZ33 Reveals Its
595   Function in Splicing and Causes Pleiotropic Changes in Development. *Mol. Biol. Cell*
596   **14**:3565–3577.

597 **Karimi, M., Inzé, D., and Depicker, A.** (2002). GATEWAY^{TM} vectors for Agrobacterium-
598   mediated plant transformation. *Trends in Plant Science* **7**:193–195.

599 **Kelemen, O., Convertini, P., Zhang, Z., Wen, Y., Shen, M., Falaleeva, M., and Stamm, S.**
600   (2013). Function of alternative splicing. *Gene* **514**:1–30.

601 **Keren, H., Lev-Maor, G., and Ast, G.** (2010). Alternative splicing and evolution:
602   diversification, exon definition and function. *Nat Rev Genet* **11**:345–355.

603   **Kleine-Vehn, J., Dhonukshe, P., Sauer, M., Brewer, P. B., Wiśniewska, J., Paciorek, T.,**
604   **Benková, E., and Friml, J.** (2008a). ARF GEF-Dependent Transcytosis and Polar
605   Delivery of PIN Auxin Carriers in Arabidopsis. *Current Biology* **18**:526–531.

606   **Kleine-Vehn, J., Łangowski, Ł., Wiśniewska, J., Dhonukshe, P., Brewer, P. B., and**
607   **Friml, J.** (2008b). Cellular and Molecular Requirements for Polar PIN Targeting and
608   Transcytosis in Plants. *Molecular Plant* **1**:1056–1066.

609   **Kleine-Vehn, J., Ding, Z., Jones, A. R., Tasaka, M., Morita, M. T., and Friml, J.** (2010).
610   Gravity-induced PIN transcytosis for polarization of auxin fluxes in gravity-sensing
611   root cells. *PNAS* **107**:22344–22349.

612   **Kleine-Vehn, J., Wabnik, K., Martinière, A., Łangowski, Ł., Willig, K., Naramoto, S.,**
613   **Leitner, J., Tanaka, H., Jakobs, S., Robert, S., et al.** (2011). Recycling, clustering,
614   and endocytosis jointly maintain PIN auxin carrier polarity at the plasma membrane.
615   *Molecular Systems Biology* **7**:540.

616   **Klepikova, A. V., Kasianov, A. S., Gerasimov, E. S., Logacheva, M. D., and Penin, A. A.**
617   (2016). A high resolution map of the Arabidopsis thaliana developmental
618   transcriptome based on RNA-seq profiling. *Plant J.* **88**:1058–1070.

619   **Kriechbaumer, V., Wang, P., Hawes, C., and Abell, B. M.** (2012). Alternative splicing of
620   the auxin biosynthesis gene YUCCA4 determines its subcellular compartmentation.
621   *Plant J.* **70**:292–302.

622   **Kumar, S., Stecher, G., Li, M., Knyaz, C., and Tamura, K.** (2018). MEGA X: Molecular
623   Evolutionary Genetics Analysis across Computing Platforms. *Molecular Biology and*
624   *Evolution* **35**:1547–1549.

625   **Langowski, L., Wabnik, K., Li, H., Vanneste, S., Naramoto, S., Tanaka, H., and Friml, J.**
626   (2016). Cellular mechanisms for cargo delivery and polarity maintenance at different
627   polar domains in plant cells. *Cell Discov* **2**:16018.

628   **Laňková, M., Humpolíčková, J., Vosolsobě, S., Cit, Z., Lacek, J., Čovan, M., Čovanová,**
629   **M., Hof, M., and Petrášek, J.** (2016). Determination of Dynamics of Plant Plasma
630   Membrane Proteins with Fluorescence Recovery and Raster Image Correlation
631   Spectroscopy. *Microscopy and Microanalysis* **22**:290–299.

632   **Leitner, J., Petrášek, J., Tomanov, K., Retzer, K., Pařezová, M., Korbei, B., Bachmair,**
633   **A., Zažímalová, E., and Luschnig, C.** (2012). Lysine63-linked ubiquitylation of
634   PIN2 auxin carrier protein governs hormonally controlled adaptation of Arabidopsis
635   root growth. *PNAS* **109**:8322–8327.

636   **Li, H.-T., Yi, T.-S., Gao, L.-M., Ma, P.-F., Zhang, T., Yang, J.-B., Gitzendanner, M. A.,**
637   **Fritsch, P. W., Cai, J., Luo, Y., et al.** (2019). Origin of angiosperms and the puzzle
638   of the Jurassic gap. *Nat. Plants* **5**:461–470.

639   **Marquez, Y., Brown, J. W. S., Simpson, C., Barta, A., and Kalyna, M.** (2012).
640   Transcriptome survey reveals increased complexity of the alternative splicing
641   landscape in Arabidopsis. *Genome Res.* **22**:1184–1195.

Marquez, Y., Höpfler, M., Ayatollahi, Z., Barta, A., and Kalyna, M. (2015). Unmasking alternative splicing inside protein-coding exons defines exitrons and their role in proteome plasticity. *Genome Res.* **25**:995–1007.

Martinière, A., Lavagi, I., Nageswaran, G., Rolfe, D. J., Maneta-Peyret, L., Luu, D.-T., Botchway, S. W., Webb, S. E. D., Mongrand, S., Maurel, C., et al. (2012). Cell wall constrains lateral diffusion of plant plasma-membrane proteins. *PNAS* **109**:12805–12810.

Mei, W., Boatwright, L., Feng, G., Schnable, J. C., and Barbazuk, W. B. (2017). Evolutionarily Conserved Alternative Splicing Across Monocots. *Genetics* **207**:465–480.

Men, S., Boutté, Y., Ikeda, Y., Li, X., Palme, K., Stierhof, Y.-D., Hartmann, M.-A., Moritz, T., and Grebe, M. (2008). Sterol-dependent endocytosis mediates post-cytokinetic acquisition of PIN2 auxin efflux carrier polarity. *Nat. Cell Biol.* **10**:237–244.

Müller, K., Hošek, P., Laňková, M., Vosolsobě, S., Malínská, K., Čarná, M., Fílová, M., Dobrev, P. I., Helusová, M., Hoyerová, K., et al. (2019). Transcription of specific auxin efflux and influx carriers drives auxin homeostasis in tobacco cells. *Plant J.* **100**:627–640.

Nakabayashi, K., Bartsch, M., Ding, J., and Soppe, W. J. J. (2015). Seed Dormancy in Arabidopsis Requires Self-Binding Ability of DOG1 Protein and the Presence of Multiple Isoforms Generated by Alternative Splicing. *PLOS Genetics* **11**:e1005737.

Nodzyński, T., Vanneste, S., Zwiewka, M., Pernisová, M., Hejátko, J., and Friml, J. (2016). Enquiry into the Topology of Plasma Membrane-Localized PIN Auxin Transport Components. *Molecular Plant* **9**:1504–1519.

O'Leary, N. A., Wright, M. W., Brister, J. R., Ciufo, S., Haddad, D., McVeigh, R., Rajput, B., Robbertse, B., Smith-White, B., Ako-Adjei, D., et al. (2016). Reference sequence (RefSeq) database at NCBI: current status, taxonomic expansion, and functional annotation. *Nucleic Acids Res.* **44**:D733-745.

Pernisova, M., Prat, T., Grones, P., Harustiakova, D., Matonohova, M., Spichal, L., Nodzynski, T., Friml, J., and Hejatko, J. (2016). Cytokinins influence root gravitropism via differential regulation of auxin transporter expression and localization in Arabidopsis. *New Phytologist* **212**:497–509.

Petrasek, J., Mravec, J., Bouchard, R., Blakeslee, J. J., Abas, M., Seifertová, D., Wisniewska, J., Tadele, Z., Kubes, M., Covanová, M., et al. (2006). PIN proteins perform a rate-limiting function in cellular auxin efflux. *Science* **312**:914–918.

Rademacher, E. H., and Offringa, R. (2012). Evolutionary Adaptations of Plant AGC Kinases: From Light Signaling to Cell Polarity Regulation. *Front. Plant Sci.* **3**.

Rakusová, H., Gallego‐Bartolomé, J., Vanstraelen, M., Robert, H. S., Alabadí, D., Blázquez, M. A., Benková, E., and Friml, J. (2011). Polarization of PIN3-dependent auxin transport for hypocotyl gravitropic response in Arabidopsis thaliana. *The Plant Journal* **67**:817–826.

683 **Rakusová, H., Abbas, M., Han, H., Song, S., Robert, H. S., and Friml, J.** (2016).
684   Termination of Shoot Gravitropic Responses by Auxin Feedback on PIN3 Polarity.
685   *Current Biology* **26**:3026–3032.

686 **Reddy, A. S. N., Marquez, Y., Kalyna, M., and Barta, A.** (2013). Complexity of the
687   alternative splicing landscape in plants. *Plant Cell* **25**:3657–3683.

688 **Remy, E., Cabrito, T. R., Baster, P., Batista, R. A., Teixeira, M. C., Friml, J., Sá-**
689   **Correia, I., and Duque, P.** (2013). A major facilitator superfamily transporter plays a
690   dual role in polar auxin transport and drought stress tolerance in Arabidopsis. *Plant*
691   *Cell* **25**:901–926.

692 **Retzer, K., Butt, H., Korbei, B., and Luschnig, C.** (2014). The far side of auxin signaling:
693   fundamental cellular activities and their contribution to a defined growth response in
694   plants. *Protoplasma* **251**:731–746.

695 **Rosquete, M. R., von Wangenheim, D., Marhavý, P., Barbez, E., Stelzer, E. H. K.,**
696   **Benková, E., Maizel, A., and Kleine-Vehn, J.** (2013). An Auxin Transport
697   Mechanism Restricts Positive Orthogravitropism in Lateral Roots. *Current Biology*
698   **23**:817–822.

699 **Roychoudhry, S., Kieffer, M., Del Bianco, M., Liao, C.-Y., Weijers, D., and Kepinski, S.**
700   (2017). The developmental and environmental regulation of gravitropic setpoint angle
701   in Arabidopsis and bean. *Sci Rep* **7**:42664.

702 **Rueden, C. T., Schindelin, J., Hiner, M. C., DeZonia, B. E., Walter, A. E., Arena, E. T.,**
703   **and Eliceiri, K. W.** (2017). ImageJ2: ImageJ for the next generation of scientific
704   image data. *BMC Bioinformatics* **18**:529.

705 **Ruzicka, K., Zhang, M., Campilho, A., Bodi, Z., Kashif, M., Saleh, M., Eeckhout, D., El-**
706   **Showk, S., Li, H., Zhong, S., et al.** (2017). Identification of Factors Required for
707   m6A mRNA Methylation in Arabidopsis Reveals a Role for the Conserved E3
708   Ubiquitin Ligase HAKAI. *New Phytol* **215**:157–172.

709 **Shang, X., Cao, Y., and Ma, L.** (2017). Alternative Splicing in Plant Genes: A Means of
710   Regulating the Environmental Fitness of Plants. *International Journal of Molecular*
711   *Sciences* **18**:432.

712 **Sibout, R., Sukumar, P., Hettiarachchi, C., Holm, M., Muday, G. K., and Hardtke, C. S.**
713   (2006). Opposite Root Growth Phenotypes of hy5 versus hy5 hyh Mutants Correlate
714   with Increased Constitutive Auxin Signaling. *PLOS Genetics* **2**:e202.

715 **Sievers, F., Wilm, A., Dineen, D., Gibson, T. J., Karplus, K., Li, W., Lopez, R.,**
716   **McWilliam, H., Remmert, M., Söding, J., et al.** (2011). Fast, scalable generation of
717   high‐quality protein multiple sequence alignments using Clustal Omega. *Molecular*
718   *Systems Biology* **7**.

719 **Soumpasis, D. M.** (1983). Theoretical analysis of fluorescence photobleaching recovery
720   experiments. *Biophysical Journal* **41**:95–97.

721 **Sprague, B. L., and McNally, J. G.** (2005). FRAP analysis of binding: proper and fitting.
722   *Trends in Cell Biology* **15**:84–91.

723 **Staiger, D., and Brown, J. W. S.** (2013). Alternative splicing at the intersection of biological
724   timing, development, and stress responses. *Plant Cell* **25**:3640–3656.

725 **Stamm, S., Ben-Ari, S., Rafalska, I., Tang, Y., Zhang, Z., Toiber, D., Thanaraj, T. A.,**
726   **and Soreq, H.** (2005). Function of alternative splicing. *Gene* **344**:1–20.

727 **Swarup, K., Benková, E., Swarup, R., Casimiro, I., Péret, B., Yang, Y., Parry, G.,**
728   **Nielsen, E., De Smet, I., Vanneste, S., et al.** (2008). The auxin influx carrier LAX3
729   promotes lateral root emergence. *Nat. Cell Biol.* **10**:946–954.

730 **Szakonyi, D., and Duque, P.** (2018). Alternative Splicing as a Regulator of Early Plant
731   Development. *Front. Plant Sci.* **9**.

732 **Tress, M. L., Abascal, F., and Valencia, A.** (2017). Alternative Splicing May Not Be the
733   Key to Proteome Complexity. *Trends in Biochemical Sciences* **42**:98–110.

734 **Tseng, Q., Duchemin-Pelletier, E., Deshiere, A., Balland, M., Guillou, H., Filhol, O., and**
735   **Théry, M.** (2012). Spatial organization of the extracellular matrix regulates cell-cell
736   junction positioning. *Proc. Natl. Acad. Sci. U.S.A.* **109**:1506–1511.

737 **Tsugeki, R., Tanaka-Sato, N., Maruyama, N., Terada, S., Kojima, M., Sakakibara, H.,**
738   **and Okada, K.** (2015). CLUMSY VEIN, the Arabidopsis DEAH-box Prp16 ortholog,
739   is required for auxin-mediated development. *Plant J.* **81**:183–197.

740 **Waldie, T., and Leyser, O.** (2018). Cytokinin Targets Auxin Transport to Promote Shoot
741   Branching. *Plant Physiol.* **177**:803–818.

742 **Willige, B. C., Ahlers, S., Zourelidou, M., Barbosa, I. C. R., Demarsy, E., Trevisan, M.,**
743   **Davis, P. A., Roelfsema, M. R. G., Hangarter, R., Fankhauser, C., et al.** (2013).
744   D6PK AGCVIII Kinases Are Required for Auxin Transport and Phototropic
745   Hypocotyl Bending in Arabidopsis. *Plant Cell* **25**:1674–1688.

746 **Zadnikova, P., Petrášek, J., Marhavý, P., Raz, V., Vandenbussche, F., Ding, Z.,**
747   **Schwarzerová, K., Morita, M. T., Tasaka, M., Hejátko, J., et al.** (2010). Role of
748   PIN-mediated auxin efflux in apical hook development of Arabidopsis thaliana.
749   *Development* **137**:607–617.

750 **Zwiewka, M., Bilanovičová, V., Seifu, Y. W., and Nodzyński, T.** (2019). The Nuts and
751   Bolts of PIN Auxin Efflux Carriers. *Front Plant Sci* **10**.